Turbofan Inlet-Radiated Broadband Acoustic Flight Effects

Ian A. Clark*, Eric H. Nesbitt†, Russell H. Thomas†, and Yueping Guo†
NASA Langley Research Center, Hampton, VA 23681 USA

This paper presents the development of a new model for the prediction of inlet-radiated turbofan broadband noise. The proposed model is developed using data from the Boeing Quiet Technology Demonstrator 2 (QTD2) and the NASA/Boeing Propulsion Airframe Aeroacoustics and Aircraft System Noise (PAA&ASN) flight tests. It is shown that, in contrast to aft-radiated noise, phased array measurements are crucial to isolate inlet-radiated noise and to capture the relevant characteristics of this noise source for modeling. The proposed model is created using data from an acoustically lined inlet, which influences the spectral shape of the model and improves performance over a wider frequency range for in-service aircraft. Directivity characteristics and throttle setting dependence are discussed. Significant improvements over prior methods implemented in the NASA Aircraft Noise Prediction Program are demonstrated, and predicted deltas to measured levels are reduced from ±10 dB to ±3 dB at the most relevant frequencies.

I. Introduction

As commercial air traffic increases, noise pollution near airports steadily becomes a more significant problem for nearby residents and businesses. Immense progress has been made over decades to reduce noise of individual flyovers, but increased demand for air travel results in more frequent flyovers and noise exposure. The NASA Advanced Air Transport Technology (AATT) project seeks to explore and develop technologies and concepts for safe, economical, energy-efficient, and quiet fixed-wing subsonic transports [1]. In order to guide future investment into concept and technology development, the project must have the capability to accurately predict noise levels of current and future aircraft. Accurate noise prediction can help identify potential airframe or engine design changes for reduced noise and can provide assurance that investment into a noise reduction technology will return real benefits in service. Although initially designed and developed in the 1970's, the NASA Aircraft Noise Prediction Program (ANOPP) has been continuously updated with improved noise models to reflect the acoustic characteristics of more recent aircraft design features. The second-generation framework, ANOPP2, provides an expanded capability set with a modern interface relative to legacy ANOPP, but much of the development focus has been on rotorcraft and propeller acoustics, in addition to universal acoustics capability such as noise propagation. As part of a larger effort to expand the capability of NASA to predict noise of commercial subsonic transports as described by Thomas et al. [2], the ANOPP2 Subsonic Transport Acoustics Research Suite (ASTARS) is in development and will include, among other methods, an improved combustor noise prediction method (see Nesbitt et al. [3]) and an improved turbofan noise prediction method, which is the subject of this paper and several prior papers [4–6]. These methods are being developed via analysis of acoustic data from several flight tests, in addition to learnings from various wind tunnel tests.

Acoustic data collected from dedicated flight tests of modern aircraft provide the best information with which to develop updated noise models. Such data provide insight into key aspects of noise generation and propagation that are not always observable in wind tunnel or static tests, such as effects of engine integration with an airframe. The Propulsion Airframe Aeroacoustics and Aircraft System Noise (PAA&ASN) flight test was performed in August 2020 in collaboration with The Boeing Company as part of the ecoDemonstrator 2020 program. The test was carefully designed for high signal-to-noise ratio and repeatability, yielding a complete dataset with which to evaluate many of the models that comprise ANOPP, including those for fan noise and liner effects. An overview of the full test campaign is presented by Thomas et al. [7] and Czech et al. [8]. Clark et al. [4] performed a first analysis of the measurements focused on fan noise and liner effects and found significant discrepancies between the measured noise and noise predicted using the method of Krejsa and Stone [9], particularly in the aft arc. Follow-on work by Clark et al. [5] developed a new framework for aft-radiated fan broadband noise, while a companion paper by Nesbitt et al. [6] did the same for inlet- and aft-radiated fan tones. This work continues this series of papers with the objective of creating an improved model for

*Research Aerospace Engineer, Aeroacoustics Branch, AIAA Senior Member, ian.a.clark@nasa.gov.
†Senior Research Engineer, Aeroacoustics Branch, AIAA Associate Fellow.

inlet-radiated fan broadband noise, which requires several unique considerations. Generally, inlet-radiated broadband noise is more difficult to isolate, as the aft-radiated broadband noise can be a significant contributor to total measured levels even at forward angles. Other unique aspects of this study will be discussed in later sections.

II. Flight Test Setup

The NASA PAA&ASN flight test was conducted in collaboration with The Boeing Company as part of their 2020 ecoDemonstrator program. Acoustic measurements were made on a newly manufactured Boeing 787-10 Etihad Airways airliner with GEnx-1B engines. For the test conditions considered in this paper, the port engine was set at a target N1C (corrected fan shaft rotation speed), while the starboard engine was kept at flight idle. Flight data recorders on board the aircraft enabled highly accurate, time-resolved aircraft state telemetry. The test site was a privately owned airfield near Glasgow, MT with no other air traffic in the vicinity. Ground-based instrumentation included eight community microphone arrays with 42 ground-board microphones in total (see Figure 1). This paper focuses primarily on the centerline microphone array, which contained eight microphones for averaging. In addition, a large phased array was placed on the runway overrun area, as seen in Figure 1. The primary array consisted of 840 microphones, and subsets of microphones formed various subarrays for improved frequency and spatial resolution. Phased array data were collected at emission angles of 60 to 120 degrees relative to the engine inlet axis, in 10-degree increments. Further details of the PAA&ASN flight test setup are provided by Czech et al. [8].

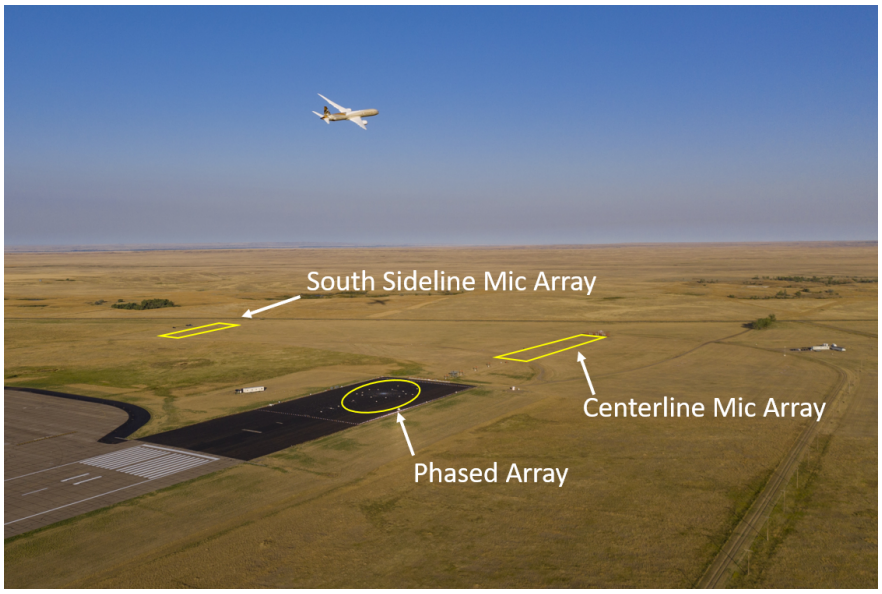

Fig. 1 Drone photograph of test aircraft flying over acoustic instrumentation. Array locations highlighted in yellow for clarity. Not all arrays are shown/highlighted. Photo credit: The Boeing Company.

During one day of flight testing, the aft duct liner was taped over to create a hardwall duct and increase the relative levels of aft-radiated noise. This assisted with the modeling efforts of Clark et al. [5] who used the hardwall data in the aft quadrant to develop a hardwall fan noise model. This ensured that the aft-radiated noise was dominant at the aft emission angles, and use of the resulting model is straightforward with a separate liner model to provide the attenuation to predict noise from a production engine. However, no such modification was made to the engine inlet as part of this flight test. This leads to several additional challenges with this study of inlet-radiated noise. First, since the inlet-radiated noise is always attenuated by the liner and tends to be less dominant than noise from the aft duct, it is more difficult to extract the relative levels of inlet-radiated contributions to total measured levels at a given emission angle. This study will make use of flight test data with the aft duct in its production (lined) configuration to minimize forward-angle contamination by aft-radiated noise. Even so, the community microphone data were found to be insufficient to adequately estimate the inlet-radiated fan noise at all but a few emission angles, which motivated the use of the phased array data. Second, a decision is required to develop a fan noise model either for the lined/treated configuration (as-measured) or for the hardwall configuration as simulated by modeling the liner attenuation and removing it from the measured data.

Both of these issues will be discussed further in Section III.

In addition to the primary dataset from the PAA&ASN flight test, data from the QTD2 flight test, conducted on a Boeing 777-300ER airplane equipped with GE90-115B engines, will also be used to supplement the analysis of fan noise. This flight test was conducted in 2005 at the same test site as the PAA&ASN flight test, with a similar setup and layout of ground-based microphone instrumentation, although only the community microphone data from that test are used in this study. Further details of the QTD2 flight test are provided by Herkes et al. [10].

III. Data Processing

A. Community Microphone Data

The community microphone data pre-processing follows a nearly identical procedure to that outlined in the previous work on aft-radiated broadband noise [5]. Tone-accurate narrowband spectra were first processed to remove the Doppler frequency shift using the precise Mach number recorded during each individual flyover and the reported emission angle for each spectrum. The spectra were then backpropagated to convert to equivalent 1 ft lossless spectra, removing the effects of spherical spreading and atmospheric absorption using the method described in ANSI S1.26-1995. Tones were filtered from the spectra using a median filter stencil method [11], followed by the minimum broadband algorithm described by Nesbitt et al. [12]. This combined algorithm yields a high-quality estimate of the broadband noise without including the broad "hay-stack" tones that are otherwise included by the median filter alone [6]. Finally, the narrowband spectra were integrated to one-third octave band spectra and calibrated to the 0.5-second integration one-third octave data.

The resulting broadband noise represented the total broadband noise measured from all sources on the aircraft, including airframe noise and engine noise sources other than fan noise. In order to isolate fan noise, a component build-up approach was used to model the spectral shape of all sources to be removed, including jet, jet-flap interaction, airframe, and combustor noise. Modeled noise was calculated for all throttle settings and emission angles. The resulting spectra were then fit to the low-frequency region of the measured data, where fan noise was expected to be a non-dominant contributor to the total levels. The fitted spectra were then subtracted from the total measured levels on a pressure-squared basis, with the result representing fan noise.

B. Dominance of Inlet-Radiated Noise

With the fan noise isolated, the next step is to consider at what emission angles the inlet noise is dominant over the aft-radiated noise, and by how much. This sets the emission angle range over which we can reliably model the noise characteristics in terms of spectral shape, amplitude, and directivity. A clue as to the dominance of the inlet noise can be obtained by considering the observed aft duct liner attenuation, computed by taking the difference in level between the hardwall and production configurations for the same engine throttle setting. Results, while not shown, indicate that some effect (>1 dB) of the aft liner is detectable even as far forward as 50 degrees. This implies that, at least for the hardwall configuration, fan noise radiated from the aft duct nozzle is a significant contributor to noise in the forward arc up to approximately 45-50 degrees. This begs the question of how the aft fan noise can be so significant at far forward angles.

To explain this, the PAA effects of fan noise are considered, especially the reflection of aft-radiated fan noise from the airframe. To compute these effects, the Propulsion Airframe Aeroacoustic Scattering (PAASc) code was used. PAASc is under development by NASA and is based on geometric acoustics and tracks the propagation of sound via rays or ray tubes through reflection and diffraction. Although the theory of geometric acoustics is well-established, PAASc incorporates many modifications and extensions to the theory for application to aircraft noise scenarios. The theoretical development is described by Guo and Thomas [13], and validation of the shielding/diffraction component of the code is described in Thomas and Guo [14]. The prediction process used for this study is a refined version of the one presented in Thomas et al. [2], also for fan broadband noise scattering by an airframe. The fan PAA effects are computed in PAASc by modeling a series of broadband point sources distributed around the inlet plane and the aft duct exit plane. To define these sources, the fan source noise is computed with the method of Krejsa and Stone [9] with the cycle parameters of the highest throttle setting, and the liner attenuation is computed with the method of Kontos [15]. The inlet and aft duct sources in PAASc are prescribed relative levels and directivities matching these results. The 787 airframe geometry was provided by Boeing to NASA and matches the configuration that was tested, namely, flaps detent 5 with landing gear stowed. The airframe geometry was discretized into a surface grid for input to PAASc. Finally, the code computed the scattering from all sources to an observer hemisphere located 800 feet from the aircraft reference

point (just below the main landing gear), with observers located every 10 degrees in both polar and azimuthal directions on the hemisphere. For this study, a slice corresponding to the flyover plane was taken to match to the results obtained by the centerline microphones. The results are then compared to the isolated engine case, where no scattering is present, to obtain an expected noise increase due to scattering PAA effects of the airframe. Further details and findings from these calculations will be described by Guo and Thomas [16].

The scattering results indicate that there is a strong correspondence (<1 dB difference) between the observed aft duct liner attenuation and the noise increase due to scattering. Detailed analysis of the PAASc results suggests that aft duct-radiated noise from the fan is reflected from the wing leading edge region, and that these reflections significantly increase the total fan noise at forward angles, even up to 50 degrees emission angle where the inlet-radiated fan noise is typically expected to be dominant. It must be emphasized that the noise increase is for the total radiated broadband fan noise, but the detailed results indicate that PAA effects were negligible for the inlet-radiated noise since there are no nearby scattering/reflecting surfaces. Therefore, the combination of results from both the aft duct liner attenuation measurement and the scattering prediction leads to the conclusion that scattering causes significant contribution of aft-radiated noise at forward angles even for the production (lined) engine, and as such, there is no angle where inlet noise can be proven to be completely dominant in the community microphone data.

C. Ground Phased Array

To move forward, the ground phased array data are critical as they provide a means to spatially isolate the inlet-radiated fan noise, such that a model can be generated for that isolated component. The conventional time series beamforming was performed by Boeing during the flight test and the results were delivered to NASA. To improve the spatial resolution and enable reliable source separation, deconvolution using DAMAS [17] was performed for one flyover at each throttle setting. This was done on a narrowband basis and the results were integrated to one-third octave bands. Next, integration regions are spatially defined within the beamform maps, and any deconvolved noise results within those regions are summed and attributed to a particular source. Separate integration regions are defined for the engine inlet and aft duct exit nozzle, and the resolution of the array after deconvolution was observed to be sufficient to separate inlet- and aft-radiated noise, even with the forward reflections of aft-radiated noise. In addition, the total spatial domain encompassing the whole aircraft is integrated so the results can be calibrated to the total ensemble-averaged, de-Dopplerized 1 ft lossless data from the community microphone array, thereby giving reliable absolute levels from the phased array. The overall process is similar to that presented in Nesbitt et al. [3].

As mentioned above, phased array data were collected every 10 degrees from 60 to 120 degrees emission angle relative to the engine axis. The results were interpolated to every 2 degrees between measurement points to match the angular resolution of the community microphones. In addition, the data were extrapolated to 30 degrees emission angle using the community microphone results; for the total levels measured at each emission angle from 30 to 60 degrees by the community microphones, it was assumed that the relative levels of the individual sources (inlet, aft, jet, etc.) were the same as at 60 degrees as extracted by the phased array. This process relies on the assumption that the directivities of the individual sources did not vary significantly from 30 to 60 degrees.

To estimate the reliability of the phased array data processing algorithm, a single repeat flyover that matched the test conditions of a high power test point was processed, and the results were compared with the original point. For context, the community microphone data showed excellent repeatability with spectral variations of much less than 1 dB, which would account for other sources of uncertainty such as variations in aircraft flight condition and position, atmospheric conditions, etc. The differences between phased array measurements at repeated test points are shown in Figure 2 for each independently processed emission angle in the forward quadrant, including 90 degrees (where the aircraft is directly overhead). In this figure, a value of 0.0 would indicate perfect repeatability between test points. As seen in the figure, the results at 60 and 70 degrees are within the expected repeatability for this type of measurement across the frequency range, with only a few deviations at 1 kHz for the 60-degree case and near 630 Hz for the 70-degree case. The results at 80 degrees show significant disparity between the two repeat runs at lower frequencies but better agreement in the mid-frequency range from approximately 1 kHz and above. Finally, the results at 90 degrees show significant degradation, with differences above 3 dB even in what should be the optimal frequency range (1-4 kHz). In this case, the relative position of the phased array with respect to the engine makes it more difficult to reliably extract noise from the inlet, especially as aft-radiated noise becomes more dominant and inlet-radiated noise is further down from the peak source in the beamform maps.

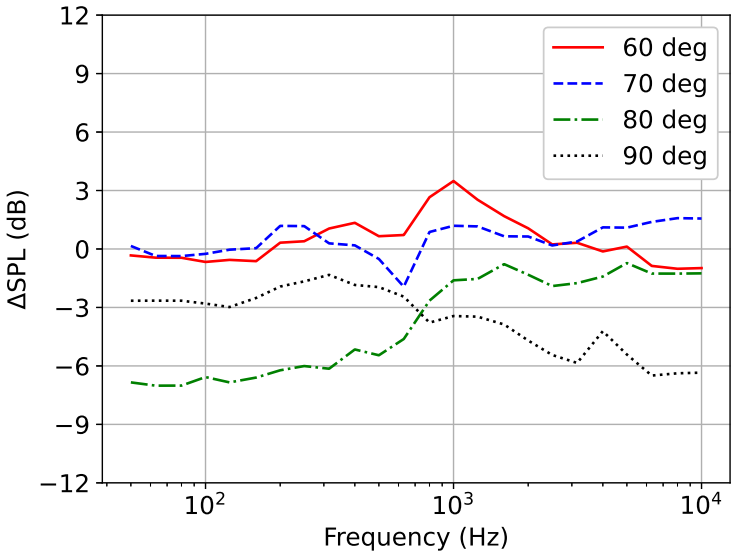

Fig. 2 Differences in phased array extracted inlet-radiated noise between repeat test points.

D. Inlet Acoustic Liner Modeling

Both the PAA&ASN 787 and the QTD2 datasets only included production (lined) inlet duct results. To create a noise model for the hardwall configuration, two approaches are possible. The first approach is to attempt to remove the liner effects, using a model such as that by Kontos et al. [15], from the measured data to recover an equivalent hardwall dataset with which to create a fan noise model. The second approach is to fit a model to the as-measured data from the treated configuration and use the liner model to adjust the resulting fan noise model for different liner treatment. As will be shown in the next section, the first approach has significant drawbacks, as the (removed) liner attenuation becomes the dominant feature of the spectra to be fitted, and the process then degrades to fitting one model to a different model. Therefore, the resulting fan noise model will be based on the treated data, and a hardwall-equivalent model can be recovered by removing the liner attenuation from the treated fan noise model. This approach is consistent with the prior work [6] on fan tones. It is important to note that a hardwall model as described here will be applicable to hardwall configurations only in the sense that applying a simple liner attenuation method such as that of Kontos et al. [15] for some given liner parameters should recover the acoustic characteristics of the lined engine of interest. However, if experimental measurements are made of a hard-walled inlet, the prediction method developed herein should not be expected to accurately predict those measured levels, as the hardwalled-inlet-radiated noise may contain contributions from certain acoustic modes that are particularly well-attenuated by the liner, such as rotor-locked modes that are barely cut-on under certain operating conditions. Combination tones, due to their non-linear propagation, are also well-attenuated by liners and will appear more prominently in hard-walled measurements than would be predicted by a method developed with this approach.

IV. Noise Modeling

The model development follows a similar process to that outlined in the previous work [5] with the functional form given in Equation 1.

$$\begin{aligned} SPL = {} & a_0 + a_1 \log_{10}(1 - M_\infty cos(\theta)) + a_2 \log_{10} A_{eff} \\ & + \beta(\theta) \log_{10} M_r + a_3 \log_{10} M_{des} \\ & + a_4 \log_{10} RSS + f_1(\theta) + f_2(f) \end{aligned} \tag{1}$$

Here, a_0 is a constant, the a_1 term corresponds to convective amplification, the a_2 term corresponds to the bypass nozzle effective area, the $\beta(\theta)$ term corresponds to the tip relative Mach number dependence, the a_3 term corresponds to the design relative tip Mach number at the Aerodynamic Design Point (ADP), and the a_4 term corresponds to the rotor stator spacing (RSS). Finally, $f_1(\theta)$ is the general directivity function and $f_2(f)$ is the spectral shape as a function

of frequency.

A. Spectral Shape

The first step to fitting the data to a model framework was fitting a spectral shape to the data. For this, the general functional form of the spectral shape function used by the Heidmann [18] framework was first considered, as shown in Eq. 2.

$$F(\eta) = 10\log_{10}\exp\left\{-0.5\left[\frac{\ln(\eta/C)}{\ln(\sigma)}\right]^2\right\} \tag{2}$$

Here, η is the frequency normalized by the blade passage frequency (since the data are de-Dopplerized), C is a constant that places the peak of the spectra at C times the blade passage frequency, and σ is a constant, set to 2.2 in the Krejsa method. However, once the results were plotted and compared with the measured data, it became apparent that this model form did not follow the trends observed in the data with regard to the frequency of the spectral peak due to several factors. First, as discussed above, with the liner attenuation removed from the measured data, the liner attenuation model dominates the shape and peak location of the spectra. While the absolute proprietary data cannot be published, this is illustrated in Figure 3. The removal of liner attenuation creates a new peak in the data at a frequency

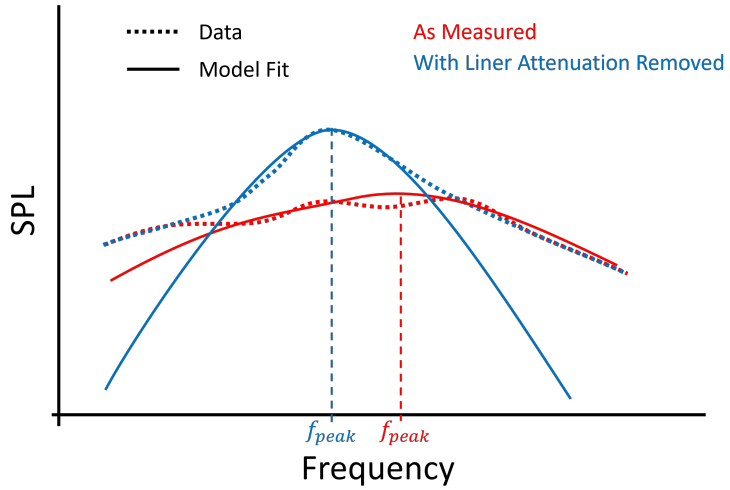

Fig. 3 Illustration of spectral fit with and without liner effects added to the measured data. The peak frequency of the spectral function is chosen to best match the data.

different than that of the measured data. To match the resulting spectral hump, a narrower model for the fan noise must be used, which degrades the agreement of the model at frequencies away from the spectral hump. In contrast, by fitting to the as-measured data with a broader spectrum, better agreement is observed over a wider range of frequencies, and removing the liner effect from this model would better recover the expected hardwall spectrum.

For evidence of this from the data, Figure 4 shows the variation of fitted spectral peak frequency (f_{peak} in Figure 3) with throttle setting, both when the liner attenuation has been removed from the data and for the as-measured treated data. To generate these plots, for each emission angle, the spectral shape function in Eq. 2 was adjusted in width to best fit the data; a new value of σ was chosen that fit both the PAA&ASN and QTD2 data well at nearly all forward emission angles. A much smaller value of σ was needed when the liner attenuation was removed, representing a narrower spectrum, while the spectrum was significantly broadened with a larger value of σ for the as-measured data. Next, the spectral shape was best fit to each individual spectrum by replacing the η parameter with frequency f, such that C becomes the peak dimensional frequency, f_{peak}, yielding Eq. 3.

$$F(\eta) = 10\log_{10}\exp\left\{-0.5\left[\frac{\ln(f/f_{peak})}{\ln(\sigma)}\right]^2\right\} \tag{3}$$

The values of f_{peak} are plotted for a range of representative emission angles as the data-fitted peaks in Figure 4. In

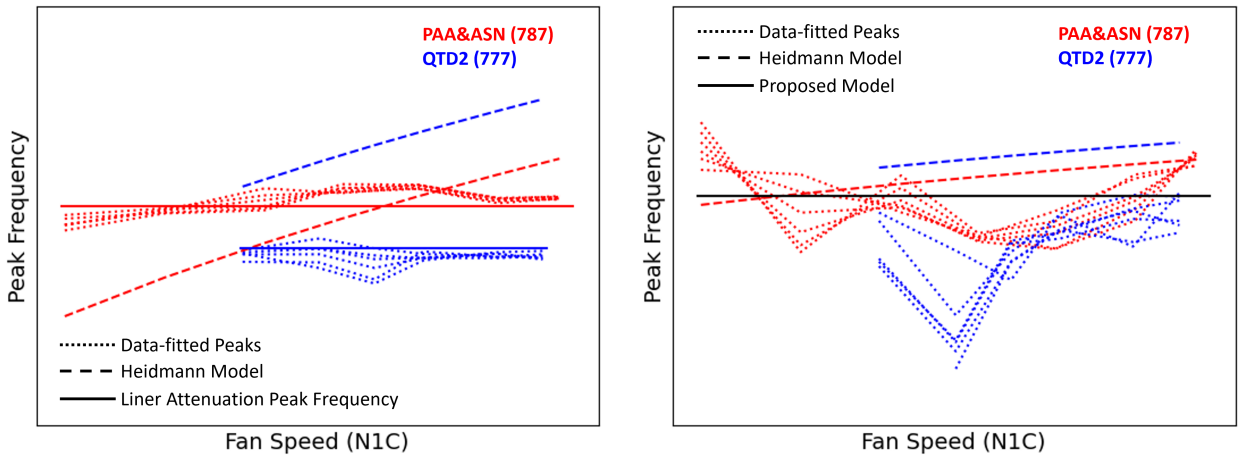

(a) Peak frequency with liner attenuation removed

(b) Peak frequency with as-measured data

Fig. 4 Spectral peak frequency vs throttle setting over a sampling of emission angles. With liner attenuation removed, the peaks are set by the modeled peak liner attenuation frequency. For the as-measured data, no clear trend is present, and a constant frequency is chosen as the spectral peak.

Figure 4a, the data-fitted peaks are nearly constant and correspond very closely to the liner attenuation peak frequency. While the Heidmann model predicts a higher peak frequency for the QTD2 data due to the high blade count and higher BPF, the larger inlet diameter of the GE90 engine on the 777 drives the liner attenuation model towards lower frequencies than for the GEnx engine on the 787. In contrast, Figure 4b shows a much wider variation in peak frequency, with no clear trend with fan speed. The wider variation in peak frequency is due in part to the wider spectral shape; small changes in peak frequency have less influence on the quality of the overall fit. It is noted that the PAA&ASN data were generated from the spectra extracted from the phased array; this was not possible with the QTD2 data, so the community mic data were used, which may explain the spurious results at lower fan speeds if contaminating sources were present. Even in this case, without the liner attenuation model factored in, the QTD2 data generally show a lower peak frequency than the PAA&ASN data, despite the higher BPF, although some overlap occurs at some fan speeds. It appears that blade passage frequency is not a suitable correlating parameter to locate the spectrum in frequency. As a data-driven improvement, Eq. 3 is used for the model, which predicts a constant peak frequency regardless of fan speed and design. A more universal treatment of this aspect of the model is certainly desired but would require additional measurements of different engines to uncover the relevant trends.

Effort was made to model the peak frequency behavior by considering the physical sources of fan broadband noise, which have been extensively studied in the literature. These sources include interaction of the inlet boundary layer with the rotor tip, interaction of the rotor wake turbulence with the stator vanes, and fan blade trailing edge noise [19]. For large fans, it is thought that the fan blade trailing edge dominates the noise generation from the fan itself [20], while impinging turbulence leads to significant noise from the stators. Morfey [21], Glegg [22], and others have correlated broadband noise frequency with the thickness of the blade wakes as they impinge on the stator vanes. The wake thickness can be related to the chord and drag coefficient of the rotor blades following the work of Wygnanski et al. [23]. Nallasamy [24] used RANS-derived parameters for the wake turbulence length scale to estimate the frequency spectrum of the turbulence impinging on the stator vanes, which was a primary input to later acoustic predictions. Unfortunately, all of these findings suggest a model that should trend in some way with fan speed, and therefore blade passage frequency, which is not seen in the data. No physical explanation for this contradiction is immediately evident, although the role of the inlet liner cannot be neglected; with the design of the engine and liner driven by (constant) certification requirements, it is reasonable to suggest that the liner design for any given engine may be tuned towards some optimal spectrum for certification. For now, this modeling effort continues assuming a constant peak frequency as shown in Figure 4b; however, this feature may be revisited before the model is finalized.

B. Throttle Setting Correlation

Following the development of a spectral model, the next step is to model the variation in level as a function of fan operating condition. As shown in prior work [4, 5], it is important to consider the variation of peak level with fan speed at each individual emission angle, such that throttle dependence and directivity are coupled in the model. The primary correlating parameter used in prior work on aft-radiated broadband noise [5] was tip relative Mach number, as given in Equation 4, and the present work continues with this approach.

$$SPL \propto \beta(\theta) \log_{10} M_r \tag{4}$$

An interesting finding of this effort was the difference in scaling behavior observed between the community microphones and the phased array. Initially, the community mics were used for both the PAA&ASN test and the QTD2 test, and in contrast to the prior study on aft-radiated noise, separate scalings were found for subsonic and supersonic tip relative Mach numbers. The data supporting this can be seen in Figure 5a, which shows the peak SPL as a function of tip relative Mach number for a selected range of emission angles near the peak radiation angle, for the PAA&ASN 787 test only. A distinct break appears near $M_r = 1$, and two well-defined slopes are observed in the subsonic and supersonic

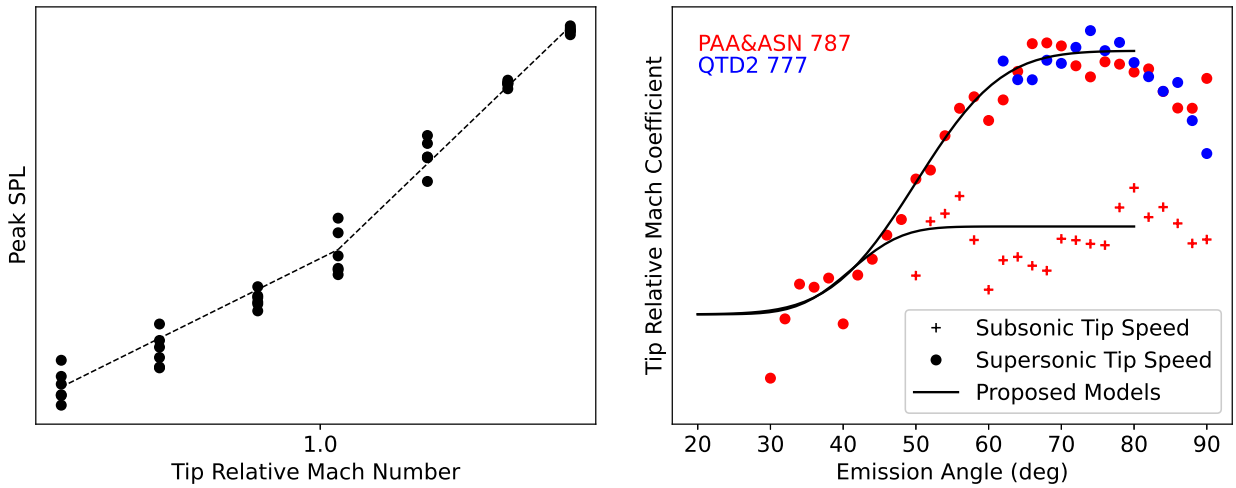

(a) Measured SPL vs Tip Relative Mach

(b) Optimized Tip Mach Coefficient vs Emission Angle

Fig. 5 Analysis of tip relative Mach number dependence with emission angle and operating condition using community microphone data.

tip regimes. Therefore, for each emission angle, the optimal coefficient $\beta(\theta)$ is computed and plotted as symbols in Figure 5b for both datasets. Note that the QTD2 777 was only operated at supersonic tip relative Mach numbers, and combination tones dominated the spectrum at far-forward emission angles (not shown). Good agreement is observed between the two datasets for the supersonic case. A smooth error function can be fit through the data separately for the subsonic and supersonic cases. Although the data clearly drive the model towards a higher coefficient (corresponding to higher sensitivity) at higher Mach numbers, this is in contrast to the findings of Nesbitt et al. [12], who observed that inlet-radiated fan broadband noise would approximately plateau at Mach numbers higher than one, which was thought to be a result of sonic blockage due to the high-speed flow through the rotor. Gliebe [25] makes a similar observation, but for a rotor-alone configuration without stator vanes.

However, when this process is repeated using the phased array data that spatially isolates the inlet noise through deconvolution and spatial integration, a much different narrative emerges. Figure 6 shows the results of the same scaling process as shown in Figure 5, but now with the phased array data from the PAA&ASN 787 flight test. Rather than a break at $M_r = 1$, the data show a consistent trend that fits well with the logarithmic scaling on M_r across the full range of conditions. Therefore, a single scaling function is valid for both subsonic and supersonic tip speed conditions, shown in Figure 6b. This finding is more consistent with the established literature. Note that the QTD2 777 data shown in Figure 6b is the same as that shown in Figure 5b and is processed from the community microphone data, as no phased array data were available for this level of analysis. The 777 data display a higher sensitivity to Mach number. It appears that, as introduced in Section III, the aft-radiated fan noise grows in dominance as throttle is increased (likely due to

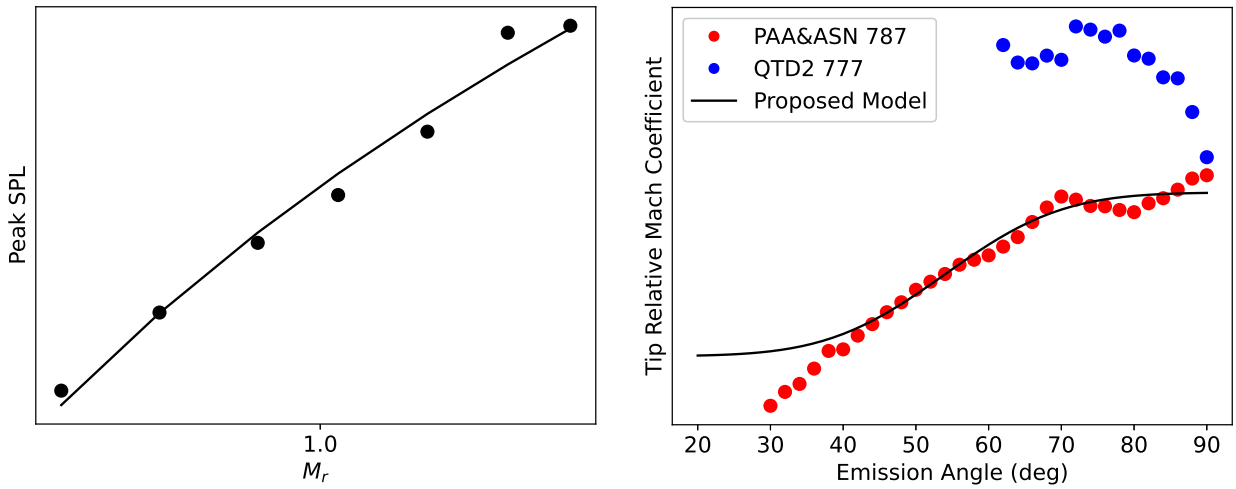

(a) Measured SPL vs Tip Relative Mach for 787

(b) Optimized Tip Mach Coefficient vs Emission Angle

Fig. 6 Analysis of tip relative Mach number dependence with emission angle and operating condition using PAA&ASN 787 phased array data, compared to QTD2 777 community microphone data.

reflection from the wing), which skews the apparent scaling in the forward quadrant. By using the phased array to filter out the contribution of aft-radiated noise, a cleaner scaling for inlet-radiated noise is obtained.

C. Directivity

With spectral shape and tip Mach number scaling set, the last major component of the overall model is directivity. The spectral peaks extracted from the last section continue to be used here. A clear trend can be observed by subtracting the other components of the model that include dependence on emission angle from the data, namely the convective amplification term and the tip Mach number dependency. The resulting dataset can be fit with a simple curve, shown in Figure 7a and compared with the previous Krejsa model. The proposed directivity function is chosen to have smoother

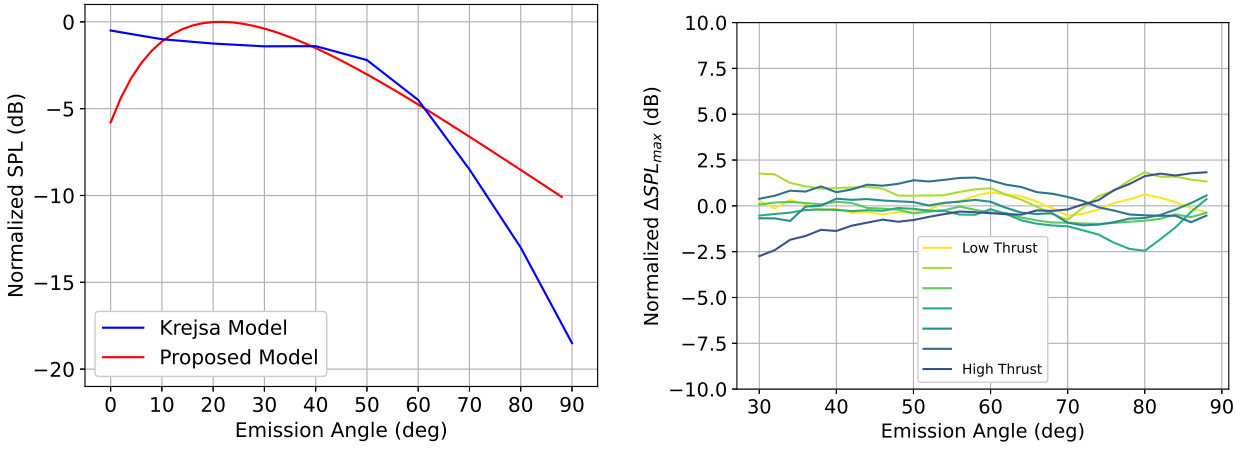

(a) Proposed directivity compared with Krejsa directivity

(b) Difference in measured and proposed directivity

Fig. 7 Proposed directivity extracted by phased array data of inlet broadband directivity.

variation than the Krejsa model, with a slight rolloff at far forward angles. Data scatter around the proposed directivity curve is within ±2.5 dB over the full range of emission angles where data are available, and within ±1.5 dB over the range of emission angles where the inlet noise was highly visible by the phased array, as seen in Figure 7b. Note that the

directivity shown here is in addition to the throttle-dependent directivity discussed in the previous section.

A critical task to complete a full model of fan broadband noise is to reconcile the directivities of inlet- and aft-radiated noise to ensure that the resulting total adds up to the measured levels at all emission angles, and especially at those angles where the two sources are approximately equal in observed amplitude. However, since the present analysis made use of phased array data that spatially isolated the inlet noise prior to modeling, the directivity shown here can be assumed to be correct for most angles. The aft directivity may need to be adjusted relative to what was used previously to generate the results of Clark et al. [5], but since the focus of this work is on inlet-radiated noise, that analysis will be left for future work once a full model is finalized and presented.

D. Final Model

The last step in the modeling process is to reconcile the two datasets (PAA&ASN 787 and QTD 777) using engine design variables, design relative tip Mach number and rotor-stator spacing, as discussed in regards to Equation 1. However, as shown in Figure 6b and discussed previously, the isolation of inlet-radiated broadband noise from the QTD2 777 dataset is unreliable, and does not likely represent the true noise characteristics of the inlet alone. Therefore, the previous coefficient for design tip Mach number is retained pending further information. Regarding rotor-stator spacing, it is noted here that Kontos et al. [26] does not utilize rotor-stator spacing for broadband noise because their prediction performed better without this parameter. Work by Woodward et al. [27, 28] showed a minimal effect of rotor-stator spacing on fan broadband noise but did reveal a modest effect of stator sweep and lean, also observed by Envia [29]. More recently, Li et al. [30] studied the effect of stator placement and orientation and found that, over a wide parameter range, broadband noise would change by less than 1 dB (their focus was on aft-radiated noise, but similar results could be expected for inlet-radiated noise). In light of this, design relative Mach number is chosen as the sole correlating parameter across engine designs, with size accounted for by fan nozzle effective area.

V. Comparison to Data

As in Clark et al. [5], the derived model is now compared to the PAA&ASN 787 data to verify that the full model behaves as expected. It is emphasized that this is a model verification, demonstrating the performance against the training data in a clear way. Model validation requires an additional, independent dataset that was not included in the model fitting procedure, and this remains for future work.

To demonstrate the improvement of the proposed model over previous models, predictions are made with the fan source noise method of Krejsa and Stone [9] and, since the inlet is acoustically lined, the liner method of Kontos et al. [15]. Spectral comparisons are shown in Figure 8 for two independent emission angles in the forward quadrant. As expected, the proposed prediction exhibits much improved agreement with the flight test data. The major features observed in the Krejsa/Kontos prediction, namely the spectral variation characterized by the dip near 2 kHz and peak near 4 kHz, are the result of the liner prediction attenuating the fan noise spectrum over a limited frequency range. In addition, the spectral shape used by the Krejsa fan noise method is narrower than that used by the proposed prediction, which results in significant underprediction at low frequencies as the spectrum drops away from the peak. In contrast, the proposed prediction method is synthesized from treated data that exhibited a smooth spectral shape, which is retained in the model. The proposed predictions also exhibit a much tighter grouping around the ideal 0-dB line, which shows that the variation with thrust setting is improved over the Krejsa formulation. The proposed prediction exhibits the best agreement with the measured data from about 700 Hz and 4 kHz, which is the most critical range for accurate Effective Perceived Noise Level (EPNL) calculation. Error grows at lower frequencies where uncertainty in phased array processing grows and at higher frequencies where noise floor issues due to atmospheric absorption and array decorrelation effects also increase uncertainty in the measured data. In general, the proposed prediction represents a strong improvement over the prior state-of-the-art methods; considering the most critical frequency range of 700 Hz to 4 kHz, the prediction delta to measurements has been reduced from approximately ±10 dB for the prior method to ±3 dB or better for the proposed method.

VI. Conclusions

An improved system-level prediction model for inlet-radiated fan broadband noise has been generated through the use of full-scale flight test data. Compared to prior formulations, the new model exhibits improved behavior across a range of engine operating conditions, emission angles, and frequencies. Discrepancies between predicted and measured levels were improved from ±10 dB with a prior model to approximately ±3 dB with the proposed model. Three unique

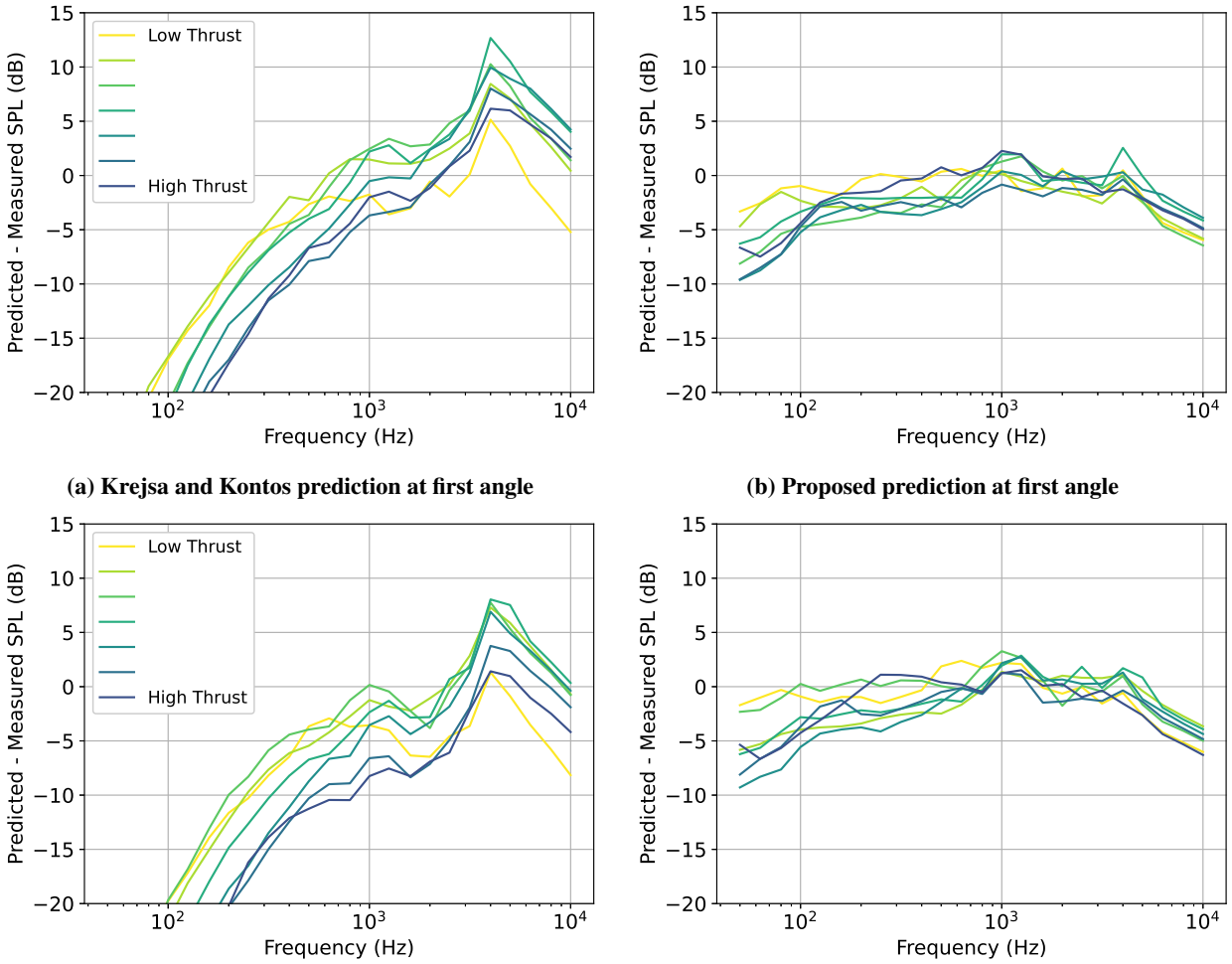

(a) Krejsa and Kontos prediction at first angle

(b) Proposed prediction at first angle

(c) Krejsa and Kontos prediction at second angle

(d) Proposed prediction at second angle

Fig. 8 Comparison of Krejsa/Kontos and proposed prediction method results with measured inlet levels extracted from phased array data.

aspects of the proposed model improve the performance relative to the previous state of the art. First, the logarithmic dependence on tip Mach number improves agreement with measured data over a wider range of engine throttle settings. Second, the coupling between directivity and throttle setting dependence improves performance at a wider range of emission angles. Finally, because the model was generated using data from a treated/lined engine inlet, it is more applicable to production aircraft. Liner configurations different from the one tested can be accounted for by computing the change in liner effect with a liner attenuation prediction model.

A key finding of this study was the need to use phased array data to spatially isolate the inlet noise from other sources of noise on the aircraft, especially aft-radiated fan noise. While it was initially expected that aft-radiated fan noise would not be dominant at forward emission angles, measurements of aft duct liner attenuation along with computations of acoustic scattering effects showed that significant aft-radiated fan noise is reflected to forward angles. This can result in erroneous scaling relationships, particularly with respect to dependence on relative tip Mach number, as the dominance of inlet- to aft-radiated noise shifts as throttle is increased.

Several aspects of the model require additional consideration in future work. First, the frequency of the spectral peak has been set in the proposed model to a constant value, regardless of fan size or design. This appears to work well for the available datasets, which are currently limited to large engines. However, additional data from various smaller engines would be advantageous to build an understanding of the dependence of this parameter. Second, because phased array data were only available for the PAA&ASN 787 test, and the QTD2 777 data exhibited unreliable isolation of

the inlet-radiated fan noise, a full model could only be created considering the 787 data. As a result of this limitation, correlation parameters could not be found to reconcile the noise model across fan designs. Coefficients from prior models were retained, but it is still necessary to verify that these coefficients hold across different aircraft in flight. Finally, work still remains to merge the model of the present study with the model for aft-radiated broadband noise and tonal noise developed in prior work.

It is emphasized here that the proposed model has been created using research-quality data from a highly relevant full-scale flight test on a state-of-the-art aircraft with modern engines, and has been shown to exhibit improved characteristics relative to prior system-level fan noise prediction methods that were developed from model-scale fan test rig data. These improvements will translate directly into improved noise predictions of current and future aircraft concepts.

Acknowledgments

The support and funding of this research by the NASA Advanced Air Transport Technology Project is gratefully acknowledged. The Boeing Company is gratefully acknowledged for the execution of the flight tests.

References

[1] *Strategic Implementation Plan, 2023 Update*, NASA Aeronautics Research Mission Directorate, 2023.

[2] Thomas, R. H., Guo, Y., Nesbitt, E. H., Clark, I. A., and June, J. C., "Refined Predictions Compared with the Propulsion Airframe Aeroacoustics and Aircraft System Noise Flight Research Test Data," *34th Congress of the International Council of the Aeronautical Sciences*, 2024. URL https://www.icas.org/ICAS_ARCHIVE/ICAS2024/data/preview/ICAS2024_0069.htm.

[3] Nesbitt, E. H., Clark, I. A., Guo, Y., and Thomas, R. H., "Far Field Combustion Noise from Full-Scale Flight Tests," *2025 AIAA Aviation Forum*, 2025.

[4] Clark, I. A., Thomas, R. H., and Guo, Y., "Fan Acoustic Flight Effects on the PAA & ASN Flight Test," *28th AIAA/CEAS Aeroacoustics Conference*, American Institute of Aeronautics and Astronautics, 2022. doi:10.2514/6.2022-2996.

[5] Clark, I., Nesbitt, E., Thomas, R. H., and Guo, Y., "Turbofan Aft-Radiated Broadband Acoustic Flight Effects," *30th AIAA/CEAS Aeroacoustics Conference*, American Institute of Aeronautics and Astronautics, 2024. doi:10.2514/6.2024-3225.

[6] Nesbitt, E., Clark, I., Guo, Y., and Thomas, R. H., "Flight Effects on Turbofan Fan Tones," *30th AIAA/CEAS Aeroacoustics Conference*, American Institute of Aeronautics and Astronautics, 2024. doi:10.2514/6.2024-3222.

[7] Thomas, R. H., Guo, Y., Clark, I. A., and June, J. C., "Propulsion Airframe Aeroacoustics and Aircraft System Noise Flight Research Test: NASA Overview," *28th AIAA/CEAS Aeroacoustics Conference*, American Institute of Aeronautics and Astronautics, 2022. doi:10.2514/6.2022-2993.

[8] Czech, M. J., Thomas, R. H., Guo, Y., June, J. C., Clark, I. A., and Shoemaker, C. M., "Propulsion Airframe Aeroacoustics and Aircraft System Noise Flight Test on the Boeing 2020 ecoDemonstrator Program," *28th AIAA/CEAS Aeroacoustics Conference*, American Institute of Aeronautics and Astronautics, 2022. doi:10.2514/6.2022-2994.

[9] Krejsa, E. A., and Stone, J. R., "Enhanced Fan Noise Modeling for Turbofan Engines," NASA/CR-2014-218421, Dec. 2014. URL https://ntrs.nasa.gov/citations/20150000884.

[10] Herkes, W. H., Olsen, R. F., and Uellenberg, S., "The Quiet Technology Demonstrator Program: Flight Validation of Airplane Noise-Reduction Concepts," *12th AIAA/CEAS Aeroacoustics Conference (27th AIAA Aeroacoustics Conference)*, American Institute of Aeronautics and Astronautics, 2006. doi:10.2514/6.2006-2720.

[11] Tukey, J. W., *Exploratory Data Analysis*, Addison-Wesley, Reading, MA, 1977.

[12] Nesbitt, E., Ganz, U., Diamond, J., and Kosanchik III, M., "An Empirical Prediction of Inlet Radiated Broadband Noise from Full Scale Engines," *36th AIAA Aerospace Sciences Meeting and Exhibit*, American Institute of Aeronautics and Astronautics, 1998. doi:10.2514/6.1998-470.

[13] Guo, Y., and Thomas, R. H., "Geometric Acoustics for Aircraft Noise Scattering," *28th AIAA/CEAS Aeroacoustics Conference*, American Institute of Aeronautics and Astronautics, 2022. doi:10.2514/6.2022-3077.

[14] Thomas, R. H., and Guo, Y., "Systematic validation of the PAAShA shielding prediction method," *International Journal of Aeroacoustics*, Vol. 21, No. 5-7, 2022, pp. 558–584. doi:10.1177/1475472x221107369.

[15] Kontos, K. B., Kraft, R. E., and Gliebe, P. R., "Improved NASA-ANOPP Noise Prediction Computer Code for Advanced Subsonic Propulsion Systems, Volume 2: Fan Suppression Model Development," NASA/CR-202309, Dec. 1996. URL https://ntrs.nasa.gov/citations/19970005047.

[16] Guo, Y., and Thomas, R. H., "Airframe Scattering of Engine Fan Noise," *To appear in International Journal of Aeroacoustics*.

[17] Brooks, T., and Humphreys, W., "A Deconvolution Approach for the Mapping of Acoustic Sources (DAMAS) Determined from Phased Microphone Arrays," *10th AIAA/CEAS Aeroacoustics Conference*, American Institute of Aeronautics and Astronautics, 2004. doi:10.2514/6.2004-2954.

[18] Heidmann, M. F., "Interim Prediction Method for Fan and Compressor Source Noise," NASA/TM X-71763, 1975. URL https://ntrs.nasa.gov/citations/19750017876.

[19] Gliebe, P. R., "Fan broadband noise - The floor to high bypass engine noise reduction," *Proceedings of Noise Con 96*, Seattle, WA, 1996, pp. 133–138.

[20] Glegg, S. A. L., and Jochault, C., "Broadband Self-Noise from a Ducted Fan," *AIAA Journal*, Vol. 36, No. 8, 1998, pp. 1387–1395. doi:10.2514/2.559.

[21] Morfey, C. L., "Broadband Sound Radiated From Subsonic Rotors," *Fluid Mech., Acoustics, and Design of Turbomachinery, Pt. 2*, NASA/SP-304, 1974. URL https://ntrs.nasa.gov/citations/19750003122.

[22] Glegg, S., "Broadband Noise from Ducted Prop Fans," *15th Aeroacoustics Conference*, American Institute of Aeronautics and Astronautics, 1993. doi:10.2514/6.1993-4402.

[23] Wygnanski, I., Champagne, F., and Marasli, B., "On the large-scale structures in two-dimensional, small-deficit, turbulent wakes," *Journal of Fluid Mechanics*, Vol. 168, 1986, pp. 31–71. doi:10.1017/s0022112086000289.

[24] Nallasamy, M., Envia, E., Thorp, S., and Shabbir, A., "Fan Noise Source Diagnostic Test - Computation of Rotor Wake Turbulence Noise," *8th AIAA/CEAS Aeroacoustics Conference and Exhibit*, American Institute of Aeronautics and Astronautics, 2002. doi:10.2514/6.2002-2489.

[25] Gliebe, P., "Observations on Fan Rotor Broadband Noise Characteristics," *10th AIAA/CEAS Aeroacoustics Conference*, American Institute of Aeronautics and Astronautics, 2004. doi:10.2514/6.2004-2909.

[26] Kontos, K. B., Janardan, B. A., and Gliebe, P. R., "Improved NASA-ANOPP Noise Prediction Computer Code for Advanced Subsonic Propulsion Systems, Volume 1: ANOPP Evaluation and Fan Noise Model Improvement," NASA/CR-195480, Aug. 1996. URL https://ntrs.nasa.gov/citations/19960048499.

[27] Woodward, R. P., and Glaser, F. W., "Wind Tunnel Measurements of Blade/Vane Ratio and Spacing Effects on Fan Noise," *Journal of Aircraft*, Vol. 20, No. 1, 1983, pp. 58–65. doi:10.2514/3.44828.

[28] Woodward, R. P., Elliott, D. M., Hughes, C. E., and Berton, J. J., "Benefits of Swept-and-Leaned Stators for Fan Noise Reduction," *Journal of Aircraft*, Vol. 38, No. 6, 2001, pp. 1130–1138. doi:10.2514/2.2883.

[29] Envia, E., "Fan Noise Source Diagnostic Test - Vane Unsteady Pressure Results," NASA/TM-2002-211808, Aug. 2002. URL https://ntrs.nasa.gov/citations/20020084621.

[30] Li, N., Winkler, J., Reimann, A. C., Voytovych, D., Mendoza, J. M., and Grace, S., "Effect of Straight and Swept FEGV Placement on Fan Broadband Interaction Noise," *30th AIAA/CEAS Aeroacoustics Conference*, American Institute of Aeronautics and Astronautics, 2024. doi:10.2514/6.2024-3161.